Heliyon 10 (2024) e27880

Contents lists available at ScienceDirect

Heliyon

journal homepage: www.cell.com/heliyon

Research article

# *In silico* molecular docking and dynamic simulation of anti-cholinesterase compounds from the extract of *Catunaregam spinosa* for possible treatment of Alzheimer's disease

Sathish Thandivel [a], Poovarasan Rajan [a], Tamizharasan Gunasekar [a], Abisek Arjunan [a], Sulekha Khute [b], Srinivasa Rao Kareti [c], Subash Paranthaman [a,*]

[a] *Department of Pharmacognosy, Sri Shanmugha College of Pharmacy, Salem district, Sankari, 637 304, Tamil Nadu, India*
[b] *Institute of Pharmacy, Pandit Ravishankar Shukla University, Raipur, 492 010, Chhattisgarh, India*
[c] *Department of Pharmacy, Indira Gandhi National Tribal University, Amarkantak, 484 887, Madhya Pradesh, India*

ARTICLE INFO

*Keywords:*
Alzheimer's disease
*In silico*
*Catunaregam spinosa*
ADMET
Acetylcholinesterase

ABSTRACT

Alzheimer's disease (AD), is characterized by a progressive loss of cognitive abilities as well as behavioral symptoms including disorientation, trouble solving problems, personality and mood changes. Acetylcholinesterase (AChE) is a promising target for symptomatic improvement in AD due to its consistent and early cholinergic deficit. This research has investigated the potential compounds from *Catunaregam spinosa* as AChE inhibitors as a treatment option for AD, aiming to enhance cholinergic neurotransmission and alleviate cognitive decline. Tacrine, the FDA's first approved treatment for AD, is no longer in use due to its hepatotoxicity. Box-Behnken design (BBD) modelling was used to optimise the ultrasonic extraction of alkaloids from the dried fruits of *C. spinosa*. GC-MS analysis revealed the presence of ninety phytoconstituents in the extract. Among them, eighty-nine new phytoconstituents are reported in this plant fruit for the first time. Out of ninety phytoconstituents, eight phytoconstituents showed the best binding affinity against the AChE enzyme, i.e., PDB IDs 1GQR, 1QTI and 4PQE of AD targets using iGEMDOCK. The lead hits were tested for their drug-like properties and atomistic binding mechanisms using *in silico* ADMET prediction, LigPlot analysis, and molecular dynamics simulation. The results suggest four compounds such as 1,4,7,10,13,16-hexaoxacyclooctadecane; butanoic acid, 3-methyl-2-[(phenylmethoxy)imino]-, trime; butane-1,2,3,4-tetraol; and D-(+)-ribonic acid.gamma-lactone as potent inhibitors of AChE for the possible treatment of AD.

## 1. Introduction

AD is a neurodegenerative disorder affecting memory, thinking, and behaviour, causing language difficulties, disorientation, mood changes, and personality changes in individuals [1]. Acetylcholine (ACh), a neurotransmitter, is rapidly hydrolyzed by the enzyme acetylcholinesterase (AChE), resulting in a reduction in acetylcholine levels and brain shrinkage, a typical clinical characteristic of AD. This loss is linked to cortical cholinergic axons and cholinoceptive neurons, while cholinesterase activity emerges in AD cortex, linked to plaques, tangles, and amyloid angiopathy. Acetylcholinesterase inhibitors (AChEI), a potentially successful therapy for AD, target

* Corresponding author.
*E-mail addresses:* subash.pharmacy@shanmugha.edu.in, subashpharm@gmail.com (S. Paranthaman).

https://doi.org/10.1016/j.heliyon.2024.e27880
Received 10 November 2023; Received in revised form 1 March 2024; Accepted 7 March 2024
Available online 20 March 2024

the breakdown of acetylcholine, a neurotransmitter crucial to memory and cognitive function [2]. The FDA approved the first generation of the Tacrine AChEIs drug in 1993, specifically designed to treat AD. However, its usage has significantly declined over the years due to concerns about its potential liver damage [3]. Additionally, the FDA has authorized several drugs to treat AD, including the NMDA antagonist memantine and the AChEIs galantamine, rivastigmine, and donepezil. These medications enhance cognitive abilities and overall quality of life, but these drugs have few short-term effects, mild to severe cholinergic side effects, and perhaps upsetting long-term toxicity [4]. As a result, other safer and more effective medications have emerged as alternatives for managing AD symptoms [5]. According to a survey, medicinal plants serve as a key source of therapy for 70–80% of rural areas and are crucial to both traditional and modern medicine. Due to their special nutritional composition, therapeutic herbs are used by a large number of disadvantaged people in developing countries, especially in rural regions [6].

*Catunaregam spinosa*, a plant in the Rubiaceae family, has long used the herb in traditional Indian medicine. *C. spinosa*, a thorny shrub or tree that may reach heights of 5–6 m, is native to Tanzania, the United States, China, India, Sri Lanka, Indonesia, Thailand, and Sri Lanka [7]. Medicinal plants supplement or substitute modern medical treatments and improve local health and security. Medicinal plants, deeply connected to social, cultural, and economic events, have been a rich source of effective and securemedicines since ancient times, treating and diagnosing diseases and infections [8]. Overall, this medicinal plant has a huge scope for CNS diseases; it has also been reported to have anti-seizure efficacy in zebrafish larvae [9] and as a CNS depressant, epilepsy, and nervine sedative [10]. Ayurveda is known as Madanaphala, its medicinal properties, include its roots, fruit, leaves, and bark, which are used in herbal remedies. The fruits, also known for their nutritional value, are also used in medicinal formulations due to their potential health-promoting properties [11]. *C. spinosa* fruit also known as mountain pomegranate, is a highly sought-after drug in Ayurveda and Unani medicine, used for sedative action, a major CNS depressant disorder [12]. It is believed to have calming effects on the nervous system and is commonly used to treat conditions such as anxiety, insomnia, and epilepsy. Additionally, the *C. spinosa* fruit is rich in antioxidants and has shown anti-inflammatory properties, making it a valuable ingredient in natural remedies for various ailments.

It contains high carbohydrates and saponins, with nutritional value mainly derived from proteins, carbohydrates, lipids, fibre, and minerals. Despite its long history, traditional Indian medicine lacks adequate scientific documentation, especially in light of modern scientific knowledge. *C. spinosa* fruit extracts exhibited the following compounds, namely 3-*O*-[β-D-glucopyranosyl-(1⟶3)-β-D-6-*O*-methyl-glucuronopyranosyl oxy]-2β-hydroxy-olean-12-en-28-oic acid; 3-*O*-[β-D-glucopyranosyl-(1 → 2)-β-D-glucopyran -osyl]-olean-12-en-28-oic acid; 3-*O*-[β-L-rhamnopyranosyl-(1 → 3)-β-D-glucuronopyranosyl- (1 → 2)-β-D-glucopyranosyl-(1 → 2)-β-D-glucopyranosyl]-12-en-28-oic acid; Oleanolic acid; 3β,2 3-dihydroxy-olean-12-ene-28-oic acid [13]. 11,14-eicosadienoic acid; palmitic acid; stearic acid; myristic acid; hexadecanoic acid; ethyl ester [14]. Seed extracts were shown the phytoconstituents like oxirane, 2,2-dimethyl-3-propyl; 2-hexene, 1-(1-ethoxyethoxy); octane, 3,6-dimethyl; heptane, 3-ethyl-2-methyl; 2-nonen-1-ol; trichloroacetic acid, 6-ethyl-3-octyl ester; nonane, 4-methyl; nonane, 2-methyl; octane, 4-ethyl; cyclohexane, 1-ethyl-2,3-dimethyl; cyclohexane, 1-methyl-2-propyl; *m*-menthane; sulfurous acid, cyclohexylmethyl octadecyl ester; decane; 3-trifluoroacetoxydodecane; octane, 1,1′-oxybis; cyclohexane, butyl; cyclopentane, pentyl; (Z)-4-decen-1-ol, methyl ether; naphthalene, decahydro-, trans; undecane; bicyclo[2.2.1] heptan-2-ol, 1,7,7-trimethyl-, (1S-endo); 9,12-octadecadienoic acid (Z,Z); hexanedioic acid, dioctyl ester; heptadecane, 9-hexyl; 1, 2-benzenedicarboxylic acid, diisooctylplasticiser; heptacosane; 2,6,10,14,18,22-tetracosahexaene,2,6,10,15,19,23-hexamethyl- [15].

Alkaloids extracted from the *Uncaria rhynchophylla* and *Palicourea deflexa*, belongs to Rubiaceae family are highlighted in research, as they shown anticholinergic activity [16,17]. Researchers are searching for alkaloids from the Rubiaceae family of *C. spinosa* to analyze the interaction between AChE enzymes using molecular modeling in an in-silico study. These alkaloids typically have nitrogen atoms in a cyclic ring like cocaine, caffeine, and nicotine, have stimulant and psychotropic effects on the CNS, potential effect of treating neurological disorders like epilepsy, psychological disorders, and AD [18]. Natural alkaloids like huperzine A and galantamine, similarly artificial substances like rivastigmine and tacrine, are examples of AChEIs. The piperidine-type AChEI donepezil differs structurally from other cholinesterase inhibitors. Alkaloids are the most promising choices for inhibiting AChE because of their complex and nitrogen-containing structures [19]. Extraction techniques for alkaloid compound-rich extracts, utilizing weight, solvent volume, and extraction time, are crucial for producing biologically active compounds from plant materials using low-cost methods [20]. The Response Surface Methodology (RSM) employs a spherical, rotating Box-Behnken response surface design to investigate process factors and responses, effectively determining optimal extraction conditions [21]. Drug design and screening often make use of *in silico* techniques (docking and dynamics), among which molecular docking is a vital technique for predicting ligand-receptor interactions. The study analyzed unbound proteins as small-world networks for docking, using various topology measures to predict ligand binding sites. The scoring stage of protein-ligand docking using the latest benchmark, and integrated into iGEMDOCK, a successful docking scoring algorithm based on physicochemical terms [22]. The human genome project has led to an increase in new molecular targets, with protein and protein-ligand complex structures solved using crystallography and nuclear magnetic resonance spectroscopy.

Additionally, computational techniques for studying ligand interactions with biological targets have improved at the atomic scale [23,24]. This study aimed to compare chemical constituents of *C. spinosa* fruit with GC-MS data and analyze secondary metabolites for anti-AD potential using *in silico* studies such as molecular docking, intermolecular interactions, ADMET predictions, and molecular dynamic simulation, which have also been performed and discussed against AChE targets. The goal was to identify new chemical components of lead molecules for AChE that are more effective than current drugs and may be targeted for treating AD.

## 2. Materials and methods

### 2.1. Chemicals

The investigation employed analytical-grade solvents such hydrochloric acid, sodium hydroxide, ethanol, and dichloromethane from Loba Chemie Pvt Ltd, Mumbai, India.

### 2.2. Plant collection

Fresh *C. spinosa* fruits were collected in June 2023 from the Sankari hills in the Tamil Nadu district of Salem. The correctness of the sample's identification and categorization was verified by the taxonomist. This voucher specimen (242-C/FRC/ID/FECC/IFGTB/2023) was placed at the Institute of Forest Genetics & Tree Breeding in Coimbatore, Tamil Nadu, India, accessible for use as a reference.

### 2.3. Extraction optimization of C. spinosa alkaloids

#### 2.3.1. Box-Behnken experimental design

In response surface technique, BBD is often used to effectively investigate the connection between many input factors and a response variable. This design is a flexible tool for process optimization and experimentation since it permits the estimation of both linear and quadratic effects [25]. The weight of the powder, the amount of the solvent, and the extraction time were the three independent variables taken into account. Examining the distinct impacts of every independent variable on the dependent variable was made possible by the single-factor analysis. This methodology yielded significant insights into the distinct roles that every component plays in the final result. By include centre points, the experimental setup's possible bias and variability are taken into consideration, resulting in a more accurate assessment of the response function. The investigation may also ascertain the degree to which random variables contribute to the overall variability in the system's performance by computing pure error. Here is how the quadratic equation is presented:

$$Y = b0 + b1X1 + b2X2 + b3X3 + b12 \times 1 \times 2 + b13 \times 1 \times 3 + b23 \times 2 \times 3 + b11X12 + b22X22 + b33X32$$

When Y is the dependent variable, the regression coefficient derived from each individual response is represented by a number between b1 and b33, while the intercept is represented by b0. The prefixed independent variables X1 (powder weight), X2 (solvent volume), and X3 (extraction time) have coded levels.

#### 2.3.2. Extraction

The samples (6 gm of dried fruit) were ground to a fine powder. Then, the plant material was mixed with 30 ml of 0.5 N HCl and placed in an ultra-sonicator bath (KLDUC-5L, Kinglab Instruments Private Limited, Tamil Nadu, India) for 60 min. The material was centrifuged for 10 min at 3000 rpm, the supernatants were mixed, and 1 N NaOH was added to bring the pH of the mixture down to 10.0. Subsequently, the organic layer was eliminated by partitioning the aqueous solution using dichloromethane. The organic layers were evaporated in a water bath, and the residue was dissolved in methanol to create a dried 0.9 % alkaloid extract from fruit powder. The resulting purified extract was ready for further analysis and characterization.

### 2.4. GC-MS instrument conditions

GC-MS analysis was performed using GCMS-QP2010 Plus (Simadzu, Toshvin Analytical Pvt. Ltd., Mumbai, India), maintaining an injection temperature of 280 °C, a solution volume of 2.0 L, and a split ratio 1: 3. The oven was preheated to 50 °C for 1 min, then to 300 °C for 10 min, with an ion source at 250 °C and pure helium inert gas. Mass spectrometry data were collected for quantitative analysis. The collected mass spectrometry data provided valuable information about the molecular weight and structure of the analyzed compounds.

### 2.5. Experimental

#### 2.5.1. Hardware specification

The study utilised an AMD Ryzen 5 5500U with a Radeon graphics processor system running on Windows 11.

#### 2.5.2. Software specifications

The ligand structures were generated using ChemDraw 19.1. PyRx 0.8 software, iGEMDOCK V2.1 for molecular docking studies, Discovery Studio Visualizer V20 for docking verifications, SMILES online translation using cactus.nci.nih.gov, AdmetSAR webserver for *in silico* investigations, and LigPlot plus V 2.1 were used to study the intermolecular interaction of receptor protein's structure. Protein-ligand complexes were solvated through by CHARMM-GUI web server. MD simulations were performed through the VMD and NAMD interface to common quantum mechanics software.

### 2.6. Preparation of the receptors

The structural receptors of AChE were obtained using the Protein Data Bank (PDB) (PDB IDs: 1GQR, 1QTI, and 4PQE). Using PyRx 0.8 software, the screening was carried out on water molecules, heteroatoms, and alternative atomic sites that were isolated from the protein receptor architectures [26].

### 2.7. Preparation of ligands

The observed ligands and tacrine were saved in PDB format, and Chem 3D 16.0 was used to reduce energy and import the ligands for accurate molecular docking studies. The MM2 force field is commonly used for energy minimization as it considers both bond lengths and angles, resulting in a more realistic representation of the ligand's conformation. By importing the ligands into the docking study workspace, their spatial orientations can be optimized for optimal binding to the target protein [27].

### 2.8. Molecular docking study

The study utilised iGEMDOCK, a docking software, to dock proteins with ligand molecules. It is a comprehensive virtual screening environment that offers user-friendly interfaces for creating the target protein binding site and screening compound library. The study utilised stable standard dock settings with 200 population sizes, 70 generations, and two solutions, selecting the optimal pose ligands based on their conformation for the lowest binding free energy. This integrated approach aids in the development of effective drug discovery strategies. This feature makes iGEMDOCK a time-saving tool for researchers as it eliminates the need for manual structure preparation, reducing the chances of errors and increasing efficiency in docking studies. Additionally, iGEMDOCK consideration of hydrogen atoms allows for a more accurate representation of the binding site, enhancing the reliability of the results obtained from docking simulations. We have created a pharmacological scoring method that allows us to separate the active compounds from screening ligands based on the pharmacological interactions. The score function for pharmacology is provided as

$$E_{(pharma)} = E_{(GEMDOCK)} + E(E)_{pharma} + 2E(H)_{pharma} + 0.5\ E(V)_{pharma}$$

where $E(E)_{pharma}$, $E(H)_{pharma}$, and $E(V)_{pharma}$ are the pharmacological scores of electrostatics, hydrogen-bonding, and vdW interactions, respectively, and EGEMDOCK is the docked energy of GEMDOCK. Finally, screening of results, iGEMDOCK offers the rankings of pharmacological and energy-based score systems [28].

### 2.9. In silico drug-likeness and ADME-tox predictions

The targetnet.scbdd.com web portal analyzed drug-likeness parameters. All seven active (higher docking score) constituents of *C. spinosa* were also evaluated using the Lipinski rule of five (RO5) [29]. The study identified potential novel molecules based on drug-likeness parameters, including molecular refractivity (MR) between 40 and 130, molecular weight (MW) not exceeding 500 gm/mol, hydrogen bond donors (HBD) not exceeding 5, hydrogen bond acceptors (HBA) not exceeding 10, and lipophilicity (log P) not exceeding 5 [30]. *In silico* ADME-Tox profiles were identified using preadmet.webservice.bmdrc.org. These profiles provided information on the pharmacokinetic properties of the potential novel molecules. The *in silico* ADME-Tox analysis helped to further narrow down the selection of molecules with favorable drug-like properties for future experimental studies. Higher docking score ligands were anlaysed the following pharmacokinetic properties like BBB, plasma protein binding energy, water solubility, and carcinogens, were recognized. These metrics allow us to assess the active ingredients of *C. spinosa* and standard tacrine that satisfy the drug-likeness and ADME-Tox requirements. This information is valuable in the development of new drugs with desirable properties.

### 2.10. LigPlot analysis

Researchers may show and assess the interactions between ligands and enzymes with the use of the useful tool LigPlot. Finding new medications and optimizing ligands for therapeutic uses are made easier with LigPlot's comprehensive information on the binding mechanism, important interactions, and spatial arrangement of the ligand. This tool generates a comprehensive diagram known as a ligand interaction plot, which offers important data about the ligand's affinity and binding process inside the receptor. Numerous interactions, including as electrostatic interactions, hydrogen bonding, hydrophobic contacts, and π-π stacking interactions, are visible in the ligand-enzyme interaction map generated by LigPlot. Additionally, the plot draws attention to specific amino acid residues in the enzymes that are engaged in these interactions; these residues are often labeled and color-coded according to the kind or intensity of the interaction [31].

### 2.11. Molecular dynamics simulation

The best-docked poses of ligands (1,4,7,10,13,16-hexaoxacyclooctadecane and butanoic acid, 3-methyl-2-[(phenylmethoxy) imino]-, trime) and standard tacrine results from the docking were used in addition to the MD simulation approach to assess the conformational space and their inhibitory potential responsible of ligand and standard drug [32–34]. Nanomolecular Dynamics (NAMD) simulation software was used for MD simulation. The CHARMM-GUI web-based platform that provides input generator, was

used to produce the ligand topology files utilizing the NAMD function input generator and the optimal binding energy ligand and standard complex with protein [35,36]. The CHARMM-GUI server was used to construct the ligand and standard topology in order to do MD simulation. After then, K+ and Cl ions were used to neutralize all of these systems by solvating them in water. Following the standard CHARMM-GUI Membrane Builder equilibration technique, these systems were reduced and proceeded through a series of equilibration phases [37]. The system was energy minimized through steepest decent steps for 1000 steps, with NVT and NPT steps processed for 100ps each during the equilibration phase, followed by 50ns MD simulation [38]. The docked ligand-target complex in order to better understand the molecular mechanism of the interactions between the enzyme and the target, enhance docking findings, and explore stability. To achieve the optimal configuration, a high-throughput dynamic simulation method must be built to study the ligand-target receptor binding process during differentiation.

## 3. Results

### 3.1. Design of experiment

Using a Box-Behnken design, the extraction yield was maximized by taking into consideration parameters such as the powder weight, the volume of the solvent, and the extraction duration. Additionally, a two-level fractional factorial design was used to investigate the primary components that influence the extraction process. The results of factorial design with independent variable into three distinct levels: −1, 0, +1 are given in Table 1. The powder weight (2–6 gm), the amount of the solvent (30–90 ml), and the extraction duration (30–90 min) were all altered in three different levels, depending on the limitations of the equipment and the moderate temperatures. All of the design tests and analyses were carried out with the help of the Design Expert 12 program, which ensured that the findings were correct. Reducing selectivity and increasing the amount of powder material both result in a considerable improvement in yield. From a weight-to-weight ratio of 0.9%, there were detected variations in yield for the optimal extraction. Response surface approach is the only important parameter that has an effect on the amount of extraction that is obtained. Response surface technique visuals are provided in Fig. 1.

### 3.2. Compound identification by GC-MS

The GC-MS analysis of *C. spinosa* extract revealed ninety phytoconstituents, which were identified and structurally elucidated using NIST 14. lib and WILEY 8. lib, based on their fragmentation patterns, allowing for both quantitative and qualitative evaluation. GC-MS chromatogram (Fig. 2) and its detected phytoconstituents were aligned according to their retention time (RT) from the fruit extract of *C. spinosa* were illustrated in supplementary table 1.

### 3.3. Identification of new compounds from C. spinosa

The GC-MS analysis identified 89 phytoconstituents in *C. spinosa* fruit, compared to the previously reported compound [12–14]. Hexadecanoic acid was the only previously reported phytoconstituent, while none of the remaining 89 were previously described as *C. spinosa* fruit constituents [13].

### 3.4. Ligand preparation

The ligands prepared from the extract of *C. spinosa* are depicted in Fig. 3 and all the ligands name described in supplementary table 1. These ligands have been extensively studied for their potential applications in various fields, including medicine and catalysis.

**Table 1**
List of dependent and independent variables in BBD.

| Std | Run | Factor 1 | Factor 2 | Factor 3 | Response 1 |
|---|---|---|---|---|---|
| | | A: Weight of powder (gm) | B: Solvent volume (ml) | C: Time (Min) | Extraction yield (%) |
| 11 | 1 | 0 | −1 | +1 | 0.7 |
| 2 | 2 | +1 | −1 | 0 | 0.82 |
| 5 | 3 | −1 | 0 | −1 | 0.78 |
| 10 | 4 | 0 | +1 | −1 | 0.5 |
| 13 | 5 | 0 | 0 | 0 | 0.62 |
| 9 | 6 | 0 | −1 | −1 | 0.54 |
| 7 | 7 | −1 | 0 | +1 | 0.45 |
| 15 | 8 | 0 | 0 | 0 | 0.62 |
| 3 | 9 | −1 | +1 | 0 | 0.7 |
| 8 | 10 | +1 | 0 | +1 | 0.6 |
| 6 | 11 | +1 | 0 | −1 | 0.45 |
| 1 | 12 | −1 | −1 | 0 | 0.8 |
| 14 | 13 | 0 | 0 | 0 | 0.58 |
| 12 | 14 | 0 | +1 | +1 | 0.45 |
| 4 | 15 | +1 | +1 | 0 | 0.45 |

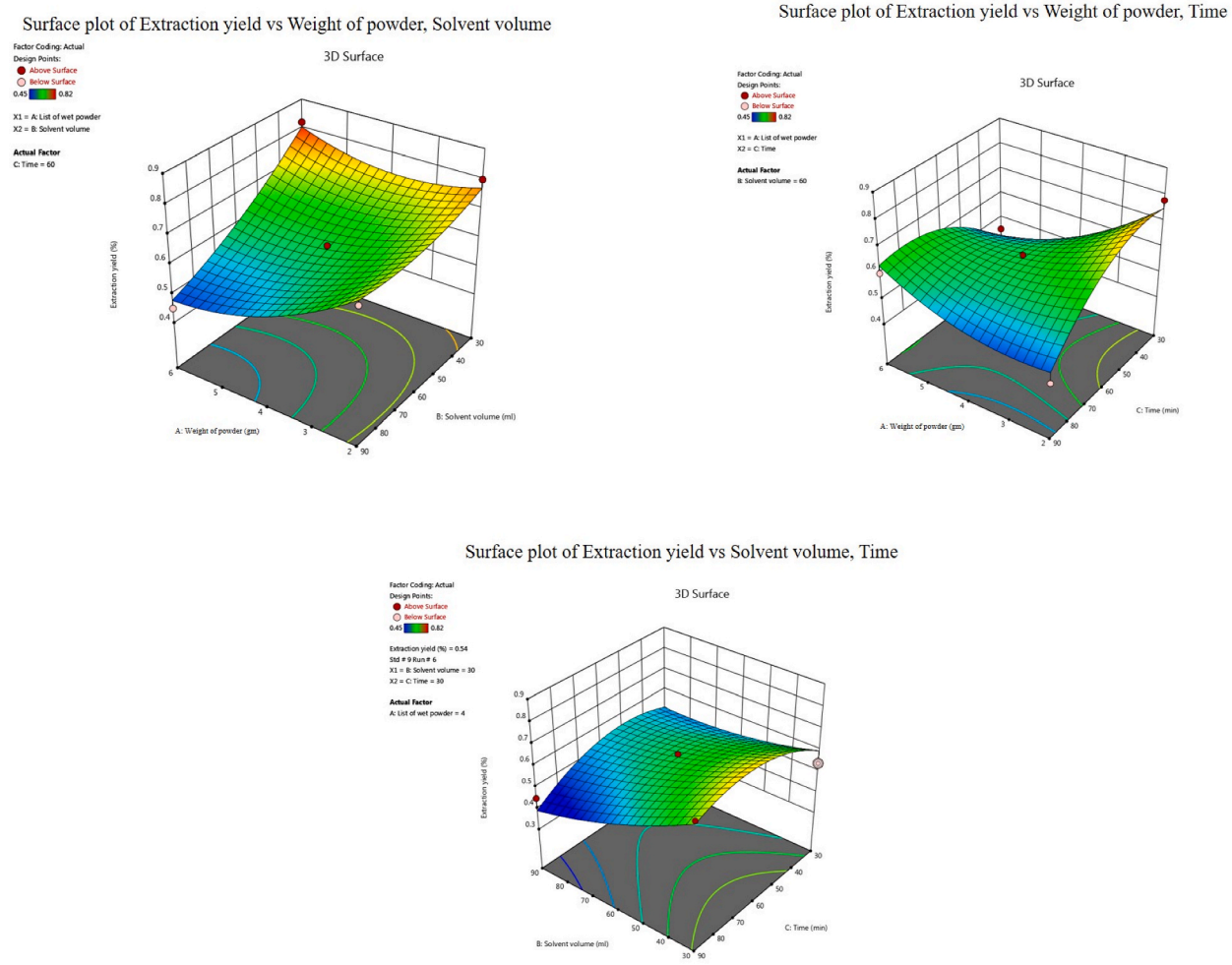


**Fig. 1.** Graphics showing the yield varying according to the different variables tested in the BBD.

### *3.5. Molecular docking study*

The analysis predicts the best-pose drugs for their interaction against AD targets of AChE. The prospective lead compounds are selected based on their greatest binding affinity with the receptors. iGEMDOCK tests demonstrate that phytocompounds from *C. spinosa* fruit extract have anti-Alzheimer's potential. supplementary table 1 illustrates the binding energy between the GC-MS-identified ligand interactions and the chosen AChE targets.

### *3.6. Top dock score phytoconstituent interaction with 1GQR*

1GQR target was shown that three compounds had docking scores greater than those of the tacrine, i.e., mome inositol (−81.4718), 1,4,7,10,13,16-hexaoxacyclooctadecane (−85.1429), and 2-[2-[2-[2-[2-[2-[2-(2-hydroxyethoxy)ethoxy]ethoxy]ethoxy]ethoxy]ethoxy]ethoxy]ethyl acetate (−80.9027).

### *3.7. Top dock score phytoconstituent interaction with 1QTI*

1QTI target was shown that seven compounds had docking scores greater than those of the tacrine, i.e., butane-1,2,3,4-tetraol -(81.2759), butanoic acid, 3-methyl-2-[(phenylmethoxy)imino]-, trime (−87.324), D-(+)-ribonic acid. gamma.-lactone (−79.6172), 1,3,4,5-tetrahydroxy-cyclohexanecarboxylic acid (−86.1999), 2,2-dimethyl-1-(trimethylsiloxy)propylidene]-[phenyl(trifluoromethyl)(trimethylsiloxy)methyl] (−79.9472), 1,4,7,10,13,16-hexaoxacyclooctadecane (−80.2894), 2-[2-[2-[2-[2-[2-[2-(2-hydroxyethoxy)ethoxy]ethoxy]ethoxy]ethoxy]ethoxy]ethoxy]ethyl acetate (−79.1069).

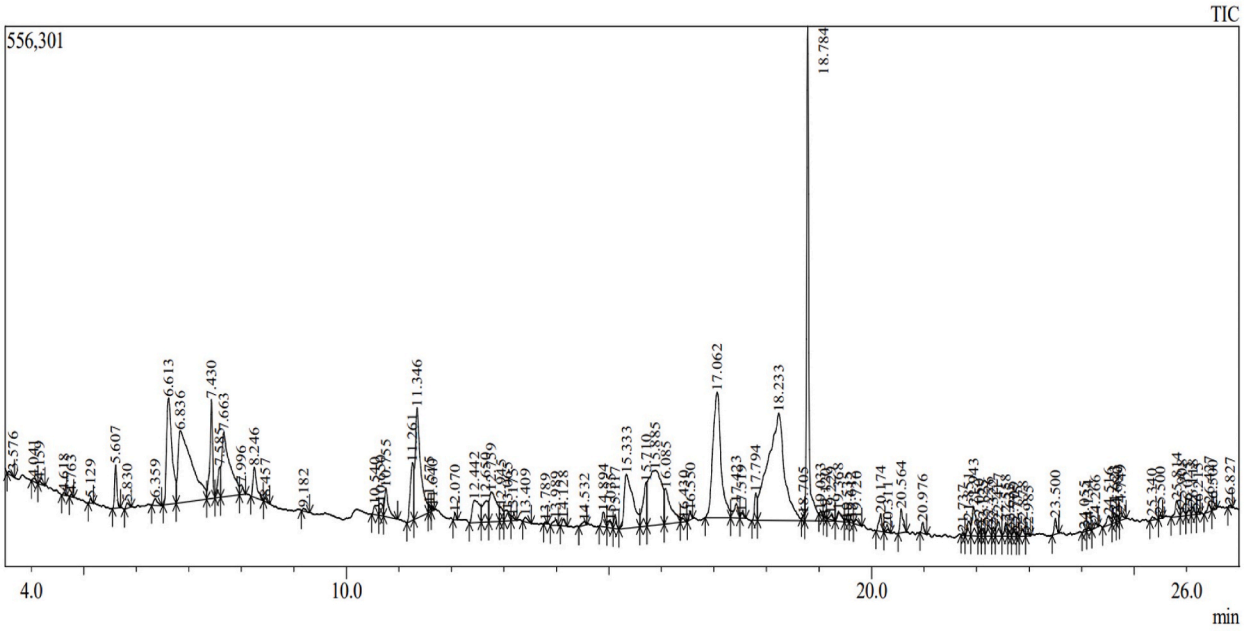


**Fig. 2.** GC-MS Chromatogram of extract of *C. spinosa* fruit.

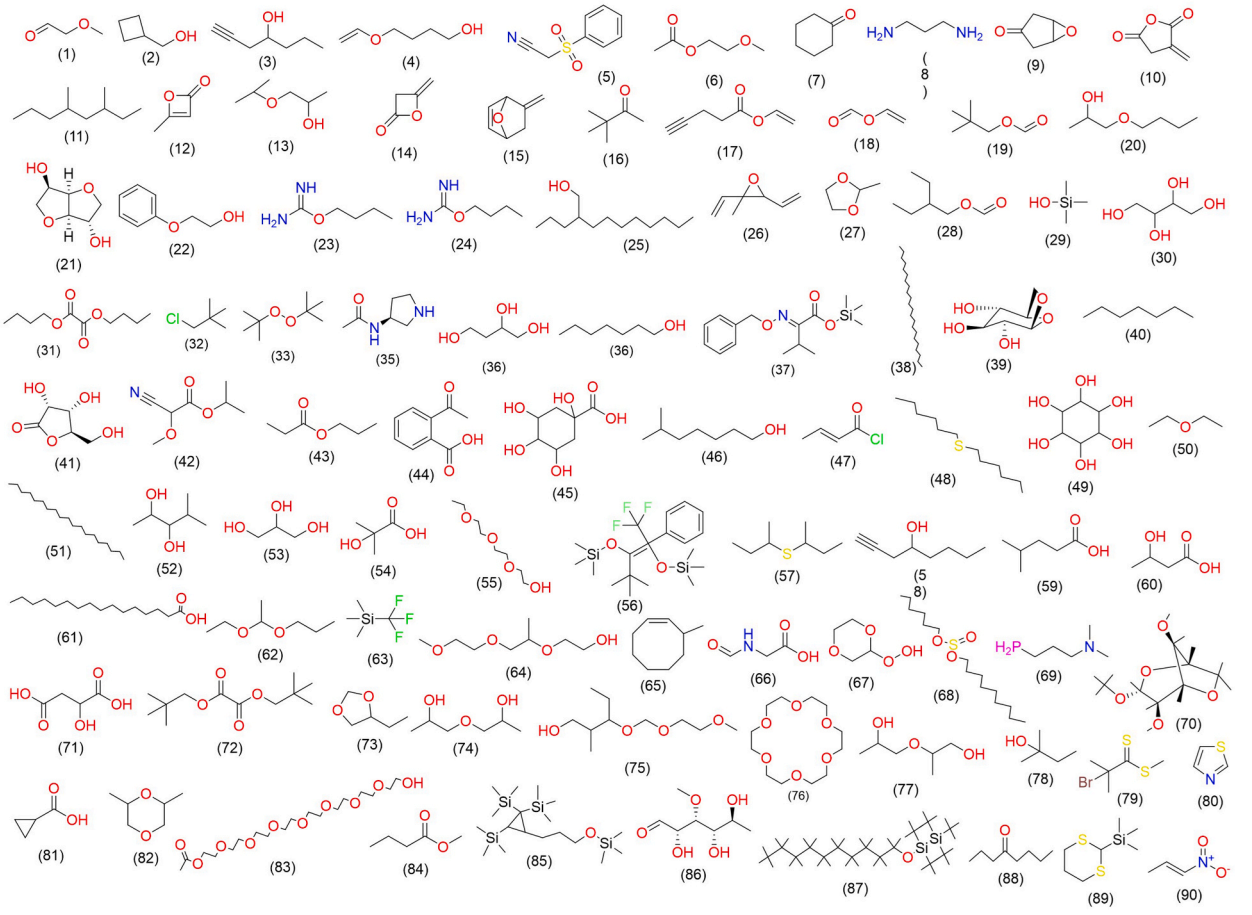


**Fig. 3.** Compounds detected in extract of *C. spinosa* by GC-MS.

### 3.8. Top dock score phytoconstituent interaction with 4PQE

4PQE target was shown that two compounds had docking scores greater than those of the tacrine, i.e., butanoic acid, 3-methyl-2-[(phenylmethoxy)imino]-, trime, (−98.3612) and 1,4,7,10,13,16-Hexaoxacyclooctadecane (−96.8495).

### 3.9. Prediction of binding sites

Hierarchical clustering of the iGEMDOCK post-screening analysis of the interaction profiles of AChE targets with the plant components of *C. spinosa* extracts and standards were presented in supplementary Fig. S1, S2 and S3. The docking chain view and 2D interactions of lead compounds and their standard with 1GQR, 1QTI and 4PQE proteins are shown in Fig. 4(a, b), Fig. 5(a, b) and Fig. 6 (a, b). Pharmacophore model shown in Fig. 7(a-f) it was generated based on the interaction of ligand and standard with the selected targets using Discovery Studio visualizer. Hydrogen bond donor is shown in pink, hydrogen bond acceptors shown in green and hydrophobic shown in gray.

### 3.10. In silico drug-likeness and ADME-tox predictions

From the docking study identified the most promising eight ligands for drug-likeness like molar refractivity, molecular weight, H-bond donor and acceptor and partition coefficient were analyzed. There were only four ligands that were passed the Lipinski's rule of five namely 1,4,7,10,13,16-hexaoxacyclooctadecane; butanoic acid, 3-methyl-2-[(phenylmethoxy)imino]-, trime; butane-1,2,3,4-tetraol and D-(+)-ribonic acid.gamma.-lactone. Similarly, these compounds were shown better ADMET properties were observed like intestinal absorption, BBB penetration, carcinogenicity, and acute oral toxicity represented in Table 2.

### 3.11. LigPlot analysis

The LigPlot analysis compared the hydrogen bond and hydrophobic interactions of *in silico* top lead hits for both the targets with their respective standards, as shown in Table 3, Fig. 8(a–f). The ligand 1,4,7,10,13,16-hexaoxacyclooctadecane with 1GQR interaction has nine hydrophobic and one H-bond interaction. Similarly, the ligand butanoic acid, 3-methyl-2-[(phenylmethoxy)imino]-, trime with 1QTI has eight hydrophobic interactions and two H-bond interactions, according to the results of LigPlot analysis for these two lead phytoconstituents from *C. spinosa*. Amino acid residues like Asp72(A), Tyr74(A), Trp84(A), Asn85(A), Ser122(A), Phe330(A), Phe331(A), Tyr334(A), His440(A) and 1 H-bond interaction Tyr121(A) were found to be forming molecular interactions 1,4,7,10,13,16-hexaoxacyclooctadecane with 1GQR, while Trp84(A), Gly118(A), Gly119(A), Phe288(A), Phe290(A), Phe331(A), Tyr334(A), His440(A), and 1 H-bond interactions Ser122(A), Tyr121(A) were observed with amino acid residues like butanoic acid, 3-

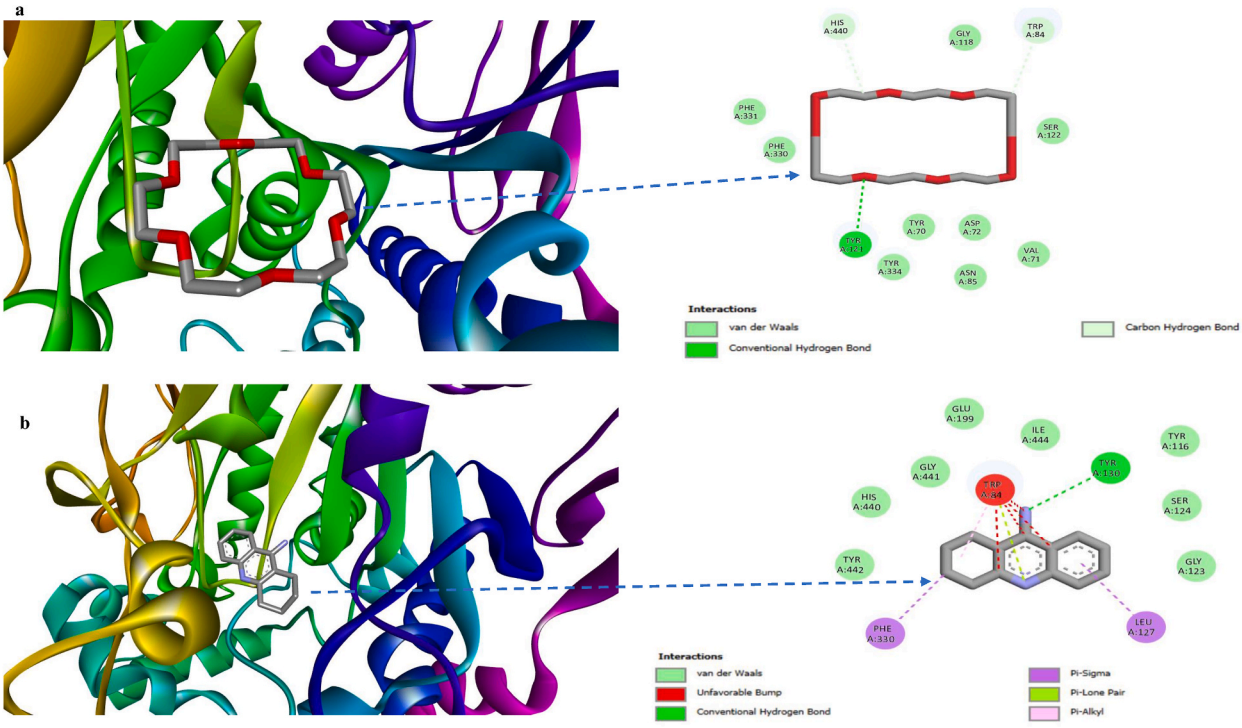


**Fig. 4.** Molecular docking view at the binding sites of 1GQR interactions: 1,4,7,10,13,16-hexaoxacyclooctadecane (a), tacrine (b).

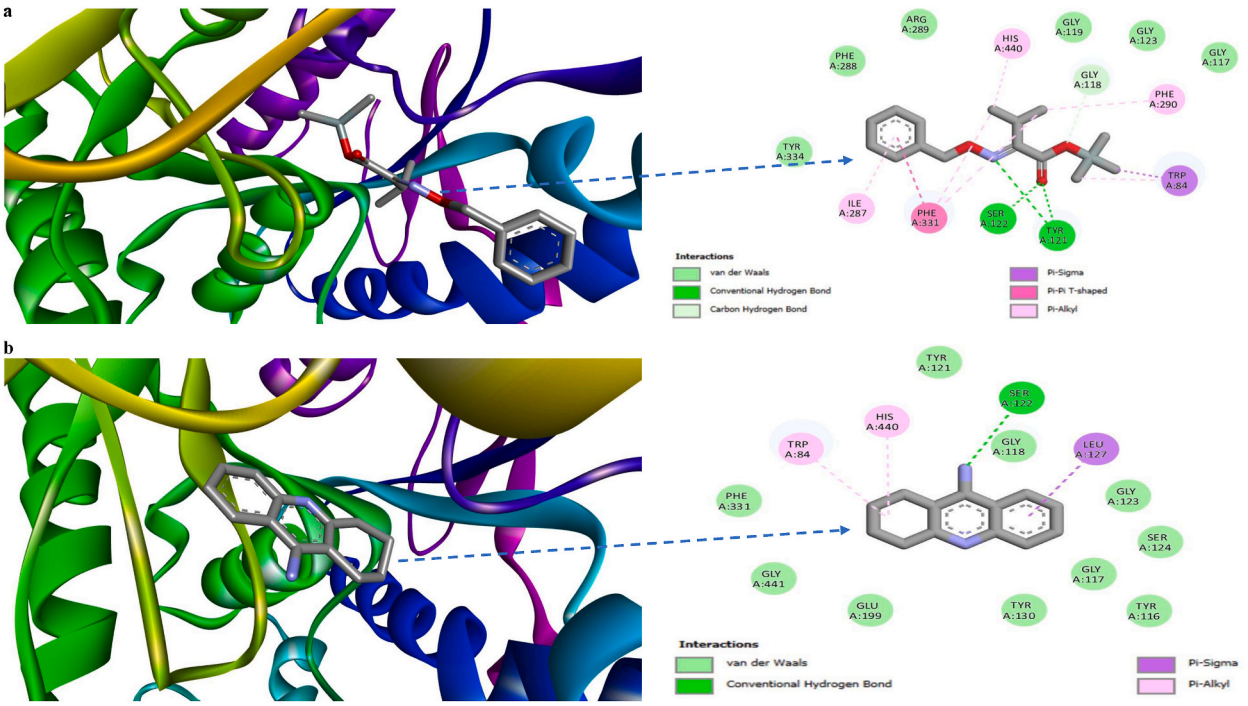


**Fig. 5.** Molecular docking view at the binding sites of 1QTI interactions: butanoic Acid, 3-methyl-2-[(phenylmethoxy)imino]-, trime (a), tacrine (b).

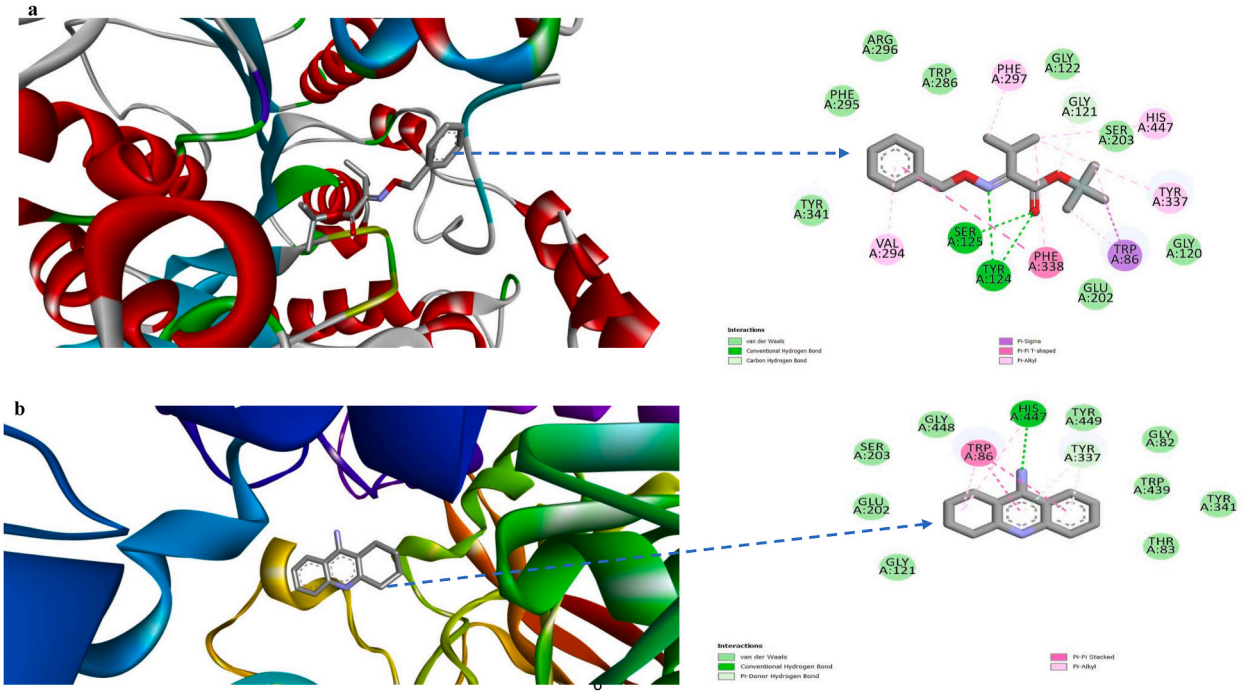


**Fig. 6.** Molecular docking view at the binding sites of 4PQE interactions: butanoic Acid, 3-methyl-2-[(phenylmethoxy)imino]-, trime (a), tacrine (b).

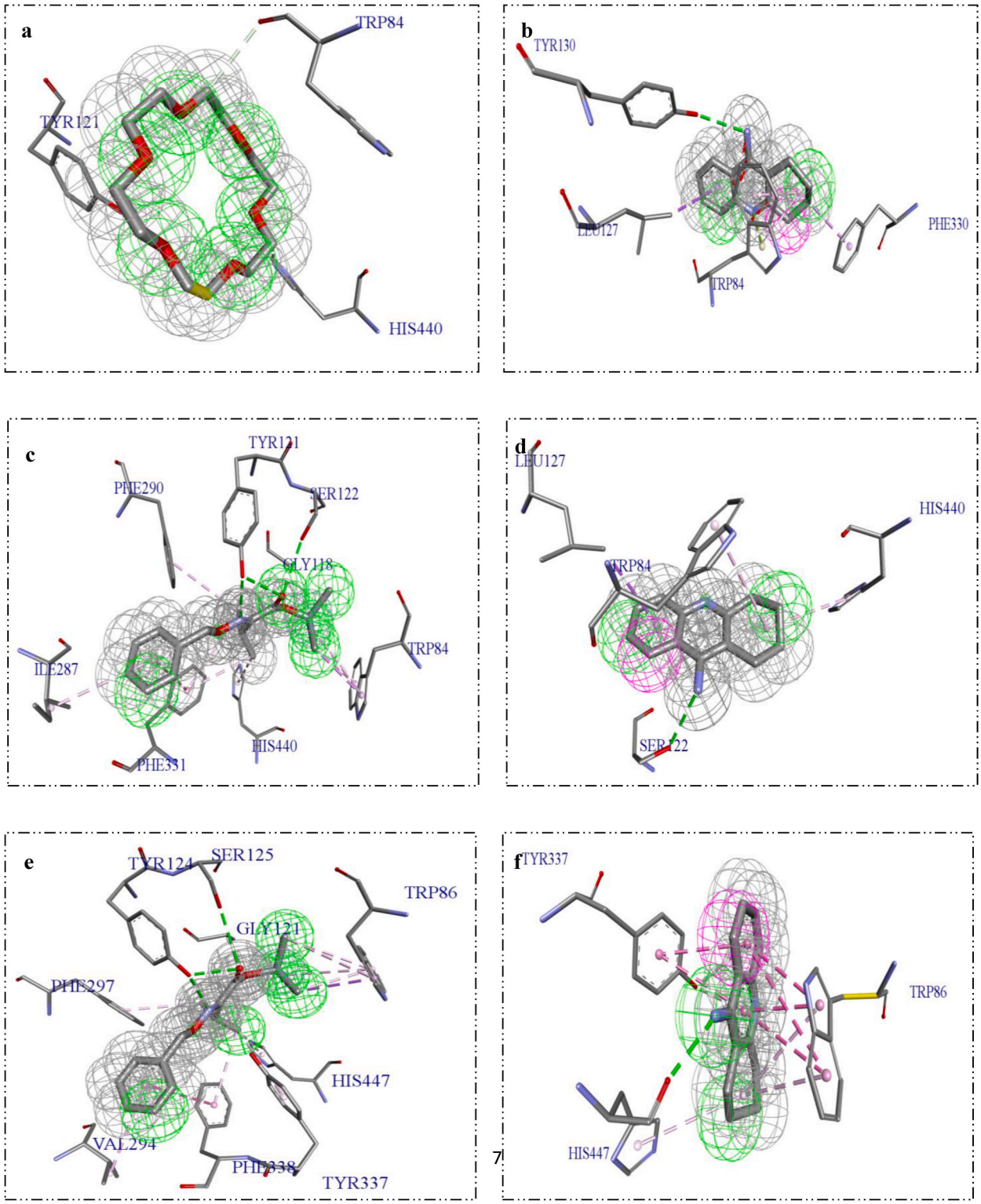


**Fig. 7.** Pharmacophore models: 1GQR interactions: 1,4,7,10,13,16-hexaoxacyclooctadecane (a), tacrine (b); 1QTI interactions: butanoic acid, 3-methyl-2-[(phenylmethoxy)imino]-, trime (c), tacrine (d); 4PQE interactions: butanoic acid, 3-methyl-2-[(phenylmethoxy)imino]-, trime (e), tacrine (f).

**Table 2**
Drug likeness and ADMET property of the selected top ligands from *C. spinosa*.

| Ligand No | Drug likeness | | | | | | ADME-Tox Profile | | | |
|---|---|---|---|---|---|---|---|---|---|---|
| | MR | MW | HBD | HBA | LogP | RO5 (%) | BBB | PPB (%) | WS | Carcino Rat |
| | 40–130 | <500 | <5 | <10 | <5 | | | | (mg/L) | |
| **Top ligands for 1GQR** | | | | | | | | | | |
| 76. | 64.194 | 264.315 | 0.0 | 6.0 | 0.099 | **100** | 0.264 | 31.276 | 343042 | -ve |
| 49. | 40.543 | 194.182 | 5.0 | 20.0 | −3.180 | 50 | 0.229 | 17.476 | 258119 | -ve |
| 83 | 98.681 | 412.472 | 1.0 | 46.0 | −0.342 | 75 | 0.028 | 33.344 | 1.368 | -ve |
| **Top ligands for 1QTI** | | | | | | | | | | |
| 37. | 83.787 | 293.433 | 0.0 | 5.0 | 3.593 | **100** | 1.273 | 94.222 | 8.394 | -ve |
| 45. | 40.106 | 192.166 | 5.0 | 6.0 | −2.321 | 75 | 0.428 | 6.595 | 1.004 | -ve |
| 30. | 25.989 | 122.119 | 4.0 | 4.0 | −2.307 | **100** | 0.096 | 85.238 | 2.322 | -ve |
| 56. | 118.014 | 438.612 | 1.0 | 5.0 | 7.485 | 75 | 1.136 | 59.371 | 9.759 | -ve |
| 41. | 28.805 | 148.114 | 3.0 | 8.0 | −2.374 | **100** | 0.267 | 67.888 | 359087 | -ve |
| **Top ligands for 4PQE** | | | | | | | | | | |
| 37. | 83.787 | 293.433 | 0.0 | 5.0 | 3.593 | **100** | 1.273 | 94.222 | 8.394 | -ve |
| 76. | 64.194 | 264.315 | 0.0 | 6.0 | 0.099 | **100** | 0.264 | 31.276 | 343042 | -ve |
| **Standard Tacrine** | | | | | | | | | | |
| – | 63.579 | 198.263 | 1.0 | 2.0 | 3.277 | 100 | 0.866 | 95.393 | 41.097 | -ve |

MR-Molar refractivity; MW- Molecular weight, HBD- Hydrogen-bond donor, HBA- Hydrogen-bond acceptor, LogP-Partition coefficient, RO5- Lipinski's rule of five, BBB-Blood-Brain-Barrier, PPB-Plasma Protein Binding and WS-Water solubility.

**Table 3**
Liplot analysis: Hydrogen bond and hydrophobic interactions of the complexes.

| S. No | Complex | Ligplot analysis | | |
|---|---|---|---|---|
| | | H-bond interactions | | Hydrophobic contacts |
| | | Amino acid | Distance (Å) | Amino acid |
| 1. | 1GQR complex with 1,4,7,10,13,16-hexaoxacyclooctadecane | Tyr121 (A) | 3.06 | Tyr70(A), Asp72(A), Trp84(A), Asn85(A), Ser122(A), Phe330(A), Phe331 (A), Tyr334(A), His440(A). |
| 2. | 1GQR complex with tacrine | Tyr130 (A) Trp84 (A) | – 3.10 | Gly123(A), Leu127(A), Phe330(A), His440(A), Gly441(A), Tyr442(A), Ile444(A). |
| 3. | 1QTI complex with butanoic acid, 3-methyl-2-[(phenylmethoxy)imino]-, trime | Ser122 (A) Tyr121 (A) | 2.96 2.72 | Trp84(A), Gly118(A), Gly119(A), Phe288(A), Phe290(A), Phe331(A), Tyr334(A), His440(A). |
| 4. | 1QTI complex with tacrine | Ser122 (A) | 3.11 | Trp84(A), Gly117(A), Gly118(A), Ser122(A), Gly123(A), Leu127(A), Try130(A), Glu199(A), His440(A). |
| 5. | 4PQE complex with butanoic acid, 3-methyl-2-[(phenylmethoxy)imino]-, trime | Tyr124 (A) Ser125 (A) | 2.76 3.30 | Trp86(A), Gly121(A), Gly122(A), Gly120(A), Glu202(A), Ser203(A), Val294(A), Phe295(A), Phe297(A), Tyr337(A), Phe338(A), Tyr341(A), His447(A). |
| 6. | 4PQE complex with tacrine | His447 (A) | 2.61 | Gly82(A), Thr83(A), Trp86(A), Glu202(A), Tyr337(A), Tyr341(A), Tyr449 (A), Trp439(A), Gly448(A). |

methyl-2-[(phenylmethoxy)imino]-, trime with 1QTI.

### *3.12. Molecular dynamics (MD) simulation*

The protein-ligand complexes with the top lead hit for both the targets (1,4,7,10,13,16-hexaoxacyclooctadecane and butanoic acid, 3-methyl-2-[(phenylmethoxy)imino]-, trime) and their standards were performed by MD simulation. The stability of the compounds to the binding site of 1GQR, 1QTI and 4PQE according to their predicted affinity. The MD simulation analyzed the behavior of proteins and ligands for 50 ns in the production phase of ligand complexes, focusing on the structure and dynamic properties of the protein-ligand complexes as backbone root-mean-squared deviation (RMSD).

To monitor conformational and structural changes of the backbone atoms of the a-amylase and protein-ligand (1,4,7,10,13,16-hexaoxacyclooctadecane; butanoic acid, 3-methyl-2-[(phenylmethoxy)imino]-, trime and tacrine) complexes were carried out by RMSD analysis and its average values were illustrated in Table 4. The RMSD plot of protein-ligand complexes (Fig. 9) was calculated for all complexes for 50 ns trajectory. In the case of the standard 1GQR – tacrine (orange) complex, the lowest average RMSD value was 0.202 nm, followed by 1QTI – tacrine (yellow) RMSD value was 0.227 nm and 4PQE-tacrine (green) RMSD value was 0.395 nm. Followed by the ligands such as, 1QTI – butanoic acid, 3-methyl-2-[(phenylmethoxy)imino]-, trime (gray) and 1GQR - 1,4,7,10,13,16-

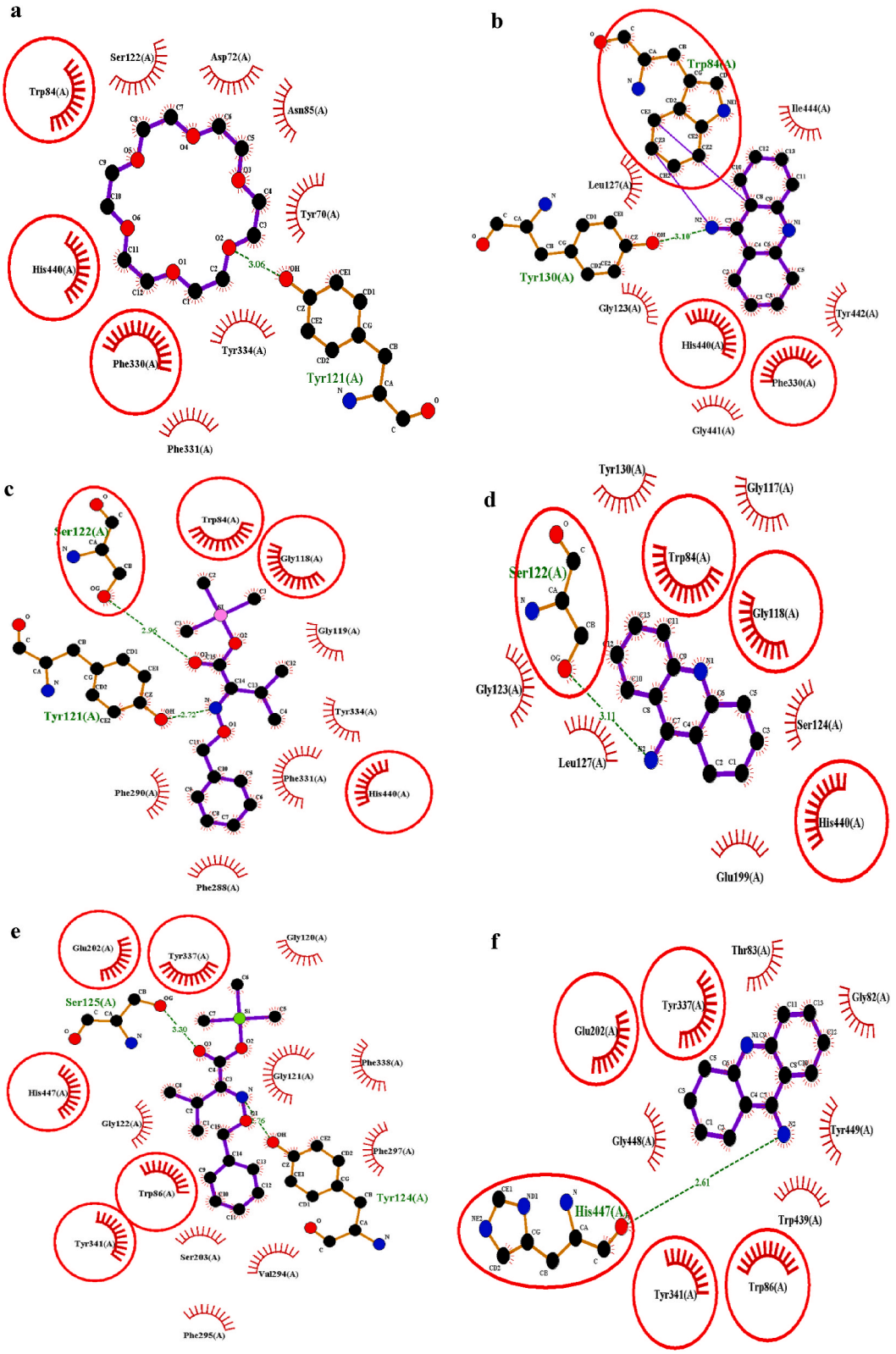


**Fig. 8.** Ligplot analysis 1GQR interactions: 1,4,7,10,13,16-hexaoxacyclooctadecane (a), tacrine (b); 1QTI interactions: butanoic acid, 3-methyl-2-[(phenylmethoxy)imino]-, trime (c), tacrine (d); 4PQE interactions: butanoic acid, 3-methyl-2-[(phenylmethoxy)imino]-, trime (e), tacrine (f).

**Table 4**
The average values of RMSD, RMSF and H bond angles in the MD simulation.

| S. No | Complex | RMSD (nm) | RMSF (nm) | H bond residue | Angle |
|---|---|---|---|---|---|
| | | Average ± SD | | | |
| 1. | 1GQR - 1,4,7,10,13,16-hexaoxacyclooctadecane | 0.245 ± 0.038 | 0.146 ± 0.068 | Tyr121 | 90.84 |
| 2. | 1GQR - tacrine | 0.202 ± 0.019 | 0.135 ± 0.068 | Tyr130 | 63.11 |
| | | | | Trp84 | 167.21 |
| 3. | 1QTI - butanoic acid, 3-methyl-2-[(phenylmethoxy)imino]-, trime | 0.244 ± 0.027 | 0.133 ± 0.081 | Tyr121 | 134.88 |
| | | | | Ser122 | 14.21 |
| 4. | 1QTI - tacrine | 0.227 ± 0.030 | 0.140 ± 0.079 | Ser122 | 34.45 |
| 5. | 4PQE - butanoic acid, 3-methyl-2-[(phenylmethoxy)imino]-, trime | 0.296 ± 0.043 | 0.159 ± 0.078 | Tyr124 | 88.44 |
| | | | | Ser125 | 16.49 |
| 6. | 4PQE - tacrine | 0.395 ± 0.049 | 0.190 ± 0.080 | His447 | 24.66 |

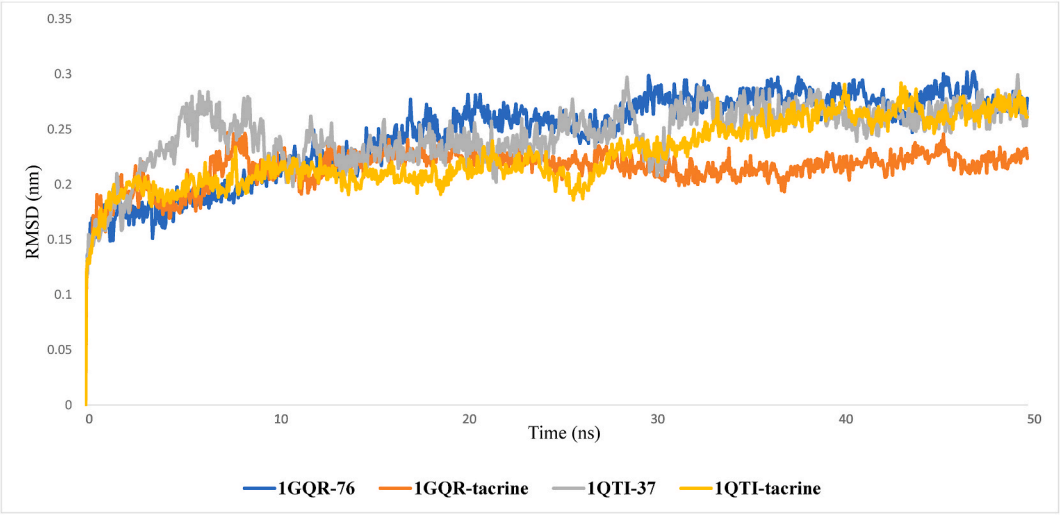


**Fig. 9.** RMSD plot of protein, standard, and ligand complex.

hexaoxacyclooctadecane (blue) and 4PQE – butanoic acid, 3-methyl-2-[(phenylmethoxy)imino]-, trime (violet) showed the highest RMSD values, i.e., 0.244, 0.245 and 0.296 nm which are also acceptable. Furthermore, the Root Mean Square Fluctuation (RMSF) analyses were performed for 1GQR, IQTI and 4PQE to evaluate the effects of its interaction with lead ligands and its standard. RMSF analysis is crucial for calculating residue fluctuations during simulation, as the RMSF value directly influences the energy of ligand-binding interaction. The higher RMSF value indicates flexible regions in the structure, while a lower value indicates a good secondary structure. The RMSF plots of ligands and standard protein complexes are depicted in Fig. 10 and the average values of RMSD, RMSF and H bond residue angles in the MD simulation were illustrated in Table 4. The results of RMSF value of standard drug indicate the 0.135, 0.140, and 0.190 nm were observed the tacrine complex with 1GQR, 1QTI and 4PQE. Similarly, the results of RMSF value the ligands indicate the 0.133, 0.146, and 0.159 nm were observed the ligand(s) complex with 1QTI – butanoic acid, 3-methyl-2-[(phenylmethoxy)imino]-, trime; 1GQR – 1,4,7,10,13,16-hexaoxacyclooctadecane and 4PQE – butanoic acid, 3-methyl-2-[(phenylmethoxy) imino]-, trime respectively. The analysis of the RMSF values clearly shows the 1GQR – 1,4,7,10,13,16-hexaoxacyclooctadecane (residues 534, 107), 1GQR – tacrine (residues 534, 535), 1QTI – butanoic acid, 3-methyl-2-[(phenylmethoxy)imino]-, trime (residues 534, 284), 1QTI – tacrine flexible region (residues 534, 535), 4PQE – butanoic acid, 3-methyl-2-[(phenylmethoxy)imino]-, trime (residues 495, 496) and 4PQE – tacrine (residue 506, 166). These findings suggest that the RMSF values vary significantly depending on the specific residues and ligands involved. Furthermore, it is evident that certain ligands, such as tacrine, have a consistent impact on the flexibility of multiple residues across different protein structures.

## 4. Discussion

More thorough clinical trials of the most promising alkaloids, the advancement of newly identified candidate alkaloids, and an ongoing search for novel alkaloids for pertinent therapeutic targets should all be part of future study [39]. The powdered fruit of *C. spinosa* was extracted using ultrasonication and methanol solvents to separate phytoconstituents. GC-MS analyses revealed 90 phytoconstituents, with 89 being the first-time detection of *C. spinosa* bark phytoconstituents. The phytoconstituents identified in AD treatment were compared with the NIST database and Wiley library. These complex inhibitors alter acetylcholine release and modulate acetylcholine receptors. Clinical trials show modest effects and frequent adverse reactions, with some drugs causing frequent reactions.

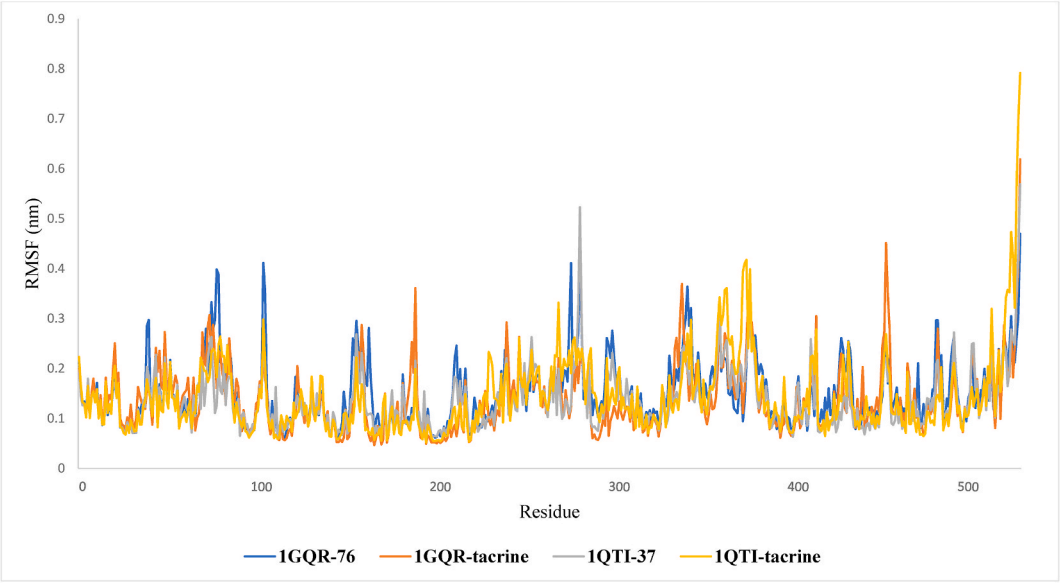


**Fig. 10.** RMSF plot of protein, standard, and ligand complex.

The pharmacological target is a crucial reason for their limited efficacy, highlighting the need for further research [40]. AChEI enhances cholinergic transmission efficiency by preventing hydrolysis of released acetylcholine, making it more accessible in the cholinergic synapse. They preserve post-synaptic muscarinic receptors in AD, with tacrine being extensively studied for their inhibitory properties [41].

GC-MS identified 90 phytoconstituents screened against three AChE targets for AD (1GQR, 1QTI and 4PQE) based on their binding affinity. We initially validated the pharmacological interactions on three therapeutic AChE protein targets for AD. The most notable structure families in the PDB collection are those that may have implications for the pharmaceutical industry. New understandings of pathology and biochemistry, however, may swiftly transform insignificant proteins into popular targets for medication treatment. The absence of structural information in structure-based virtual screening techniques is a challenge for the development and validation of methods evaluating biological activity spectrum. Although a number of structure-based strategies and algorithms for multitarget screening have been put forward, the majority of research has focused on how well they work with targets and target families that are structurally well-characterized, such as protein-ligand docking techniques [42,43].

New naphthalene derivative and citronellal are promising candidates against AChE inhibitors for AD treatment confirmed through *in silico* and *in vivo* validation [44,45]. Hydrogen bonds are crucial for protein folding, structure, and molecular recognition. Aromatic side-chains prefer binding sites, and hydrophobic and polar residues cluster at interfaces. This bonding is essential for molecular recognition, providing connection specificity and directionality. Optimal hydrogen bonding energetics and kinetics ensure stable protein structures and selectivity for targeted interactions [46,47]. The findings of docking indicate that the resulting pharmacological interactions are often necessary for the ligand to attach to the target or for the target to continue to function biologically. Additionally, a post-screening analysis module from iGEMDOCK is offered; this module is helpful in classifying compounds and presenting interaction profiles that illustrate the pharmacological interactions. For the purpose of discovering new drugs and figuring out crucial residues and interactions to comprehend binding processes, iGEMDOCK is helpful [48]. iGEMDOCK is an interactive tool that prepares the binding region of a target protein and screens chemical libraries, which has been previously reported for AD targets [49,50]. The molecular docking process was conducted in recent publication using the crystal structure of AChE from *Torpedo californica* and *Homo sapiens* with PDB IDs 1GQR, 1QTI and 4PQE [51,52]. The researchers utilised these crystal structures to predict the binding affinity and interaction between AChE inhibitors and the active site of the enzyme. The results obtained from this molecular docking study provided valuable insights into the potential therapeutic applications of these inhibitors for AD. Three phytoconstituents had the least binding energy against 1GQR, and seven had the least binding energy against 1QTI. Two compounds were common for both targets, namely 1,4,7,10,13,16-hexaoxacyclooctadecane (−85.1429) and 2-[2-[2-[2-[2-[2-[2-(2-hydroxyethoxy)ethoxy]ethoxy]ethoxy]ethoxy]ethoxy]ethoxy]ethyl acetate. Recent drug discovery relies on drugs with good pharmacokinetic properties, which must be optimized to pass standard clinical trial criteria. By optimizing these pharmacokinetic factors, researchers can ensure that the drug is effectively delivered to its target site and remains in the body for a sufficient duration to exert its therapeutic effects. Additionally, drugs with favorable pharmacokinetic properties are more likely to have predictable and manageable side effects, enhancing their safety profile during clinical trials.

The most promising phytoconstituents with the best AChE target docking score are then further screened for drug-likeness and ADME-tox prediction. The top possible three phytoconstituents that were tested for the 1GQR target revealed that one out of the three compounds, i.e., 1,4,7,10,13,16-hexaoxacyclooctadecane is a promising compound confirmed through docking analysis. The top possible five phytoconstituents tested for the 1QTI target revealed that three out of the five compounds are promising compounds

confirmed through docking analysis. i.e., butanoic acid, 3-methyl-2-[(phenylmethoxy)imino]-, trime; butane-1,2,3,4-tetraol and D-(+)-ribonic acid.gamma.-lactone. These four compounds (lead hits) passed the RO5 test and showed better BBB permeation, plasma protein binding, water solubility, and no carcinogens in rats. Moreover, our approach takes into account the possibility that a common binding site between ligand and standard drug interacting with AChE target from *Torpedo californica* and *Homo sapiens*. LigPlot analysis found both the PDB IDs having common binding site i.e., His440(A), Leu127(A), Ser122(A), Trp84(A) and Tyr334(A). However, our latest data strongly suggests that both interactions are attributed to a common binding site.

Molecular dynamics simulation of 1QTI – butanoic acid, 3-methyl-2-[(phenylmethoxy)imino]-, trime and 1GQR – 1,4,7,10,13,16-hexaoxacyclooctadecane shows the nearest RMSD and RMSF value of standard protein complexes, which indicates its stability is equivalent to the respective standard. For each system, the ring atom locations in the docked ligands and the equivalent positions in the crystallographic co-complexes were calculated, and the result was the RMSD. Posing with an RMSD of 0.2 nm or less was deemed appropriate [53]. The typical complex RMSD values for the 1GQR and 1QTI ligands were detected at 5 ns, and they stabilized with a deviance between 0.2 and 0.4 nm until the simulation's conclusion, showing high stability. The 4PQE – tacrine complex and 4PQE – butanoic acid, 3-methyl-2-[(phenylmethoxy)imino]-, trime showed higher fluctuations between 0.05 and 50ns. These oscillations are thought to be caused by ligand adjustments in the receptor binding site, structural modifications in flexible protein areas, and conformational switching brought on by bond rotations [54,55]. To forecast the local conformational changes in the protein chain and the ligands, the RMSF is crucial [56,57]. In contrast to those with high RMSF values, structures with lower RMSF values often indicate the existence of secondary structures and are also thought to be superior [58]. The average RMSF of complex all the ligands and standard were shown the range between 0.133 and 0.190 nm, respectively, which suggested the stable nature of drug-protein complexes during simulation. This indicates that the ligands and standard remained tightly bound to the protein throughout the simulation, demonstrating their strong interaction and stability. The low RMSF values further support the reliability of the results obtained from the drug-protein complex simulations.

Thus, these four phytoconstituents such as 1,4,7,10,13,16-hexaoxacyclooctadecane, butanoic acid; 3-methyl-2-[(phenylmethoxy)

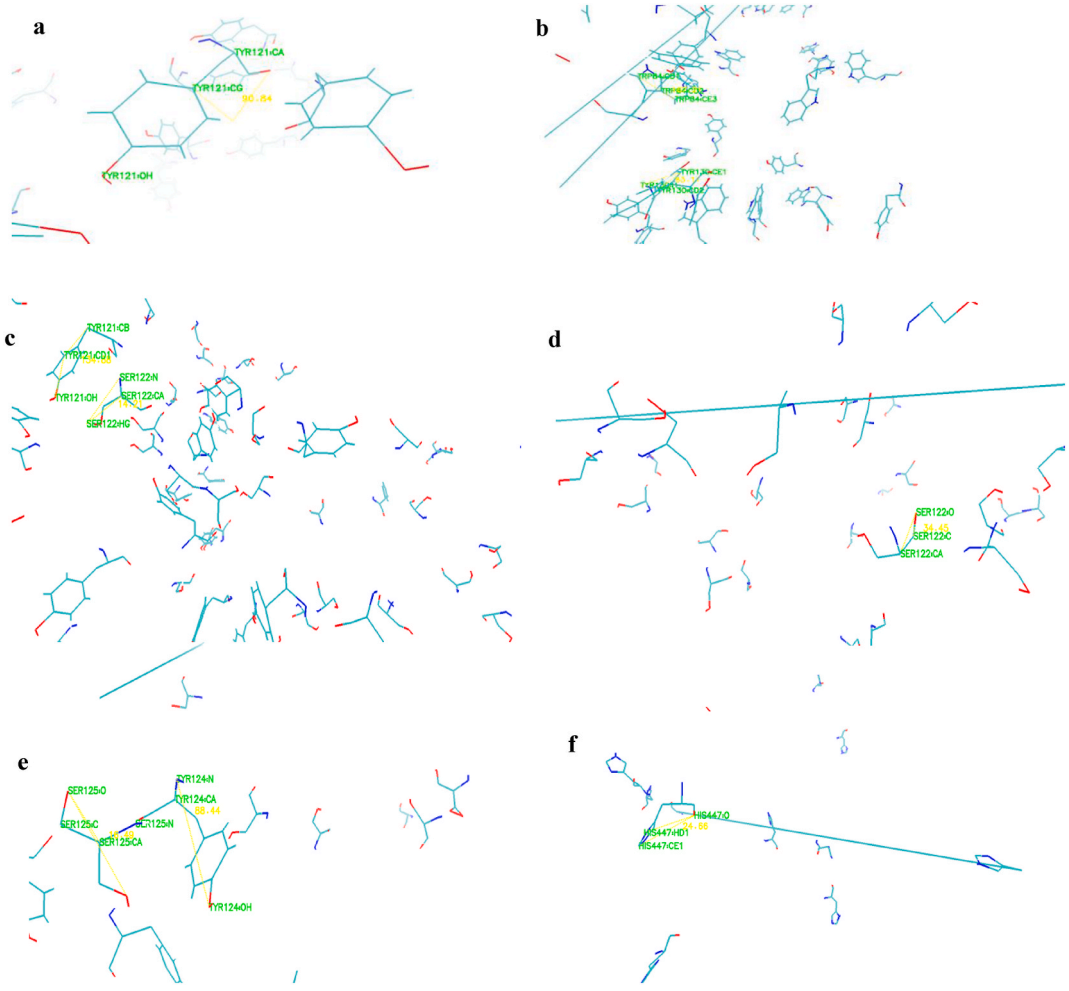


**Fig. 11.** H bond angles in the MD simulations.

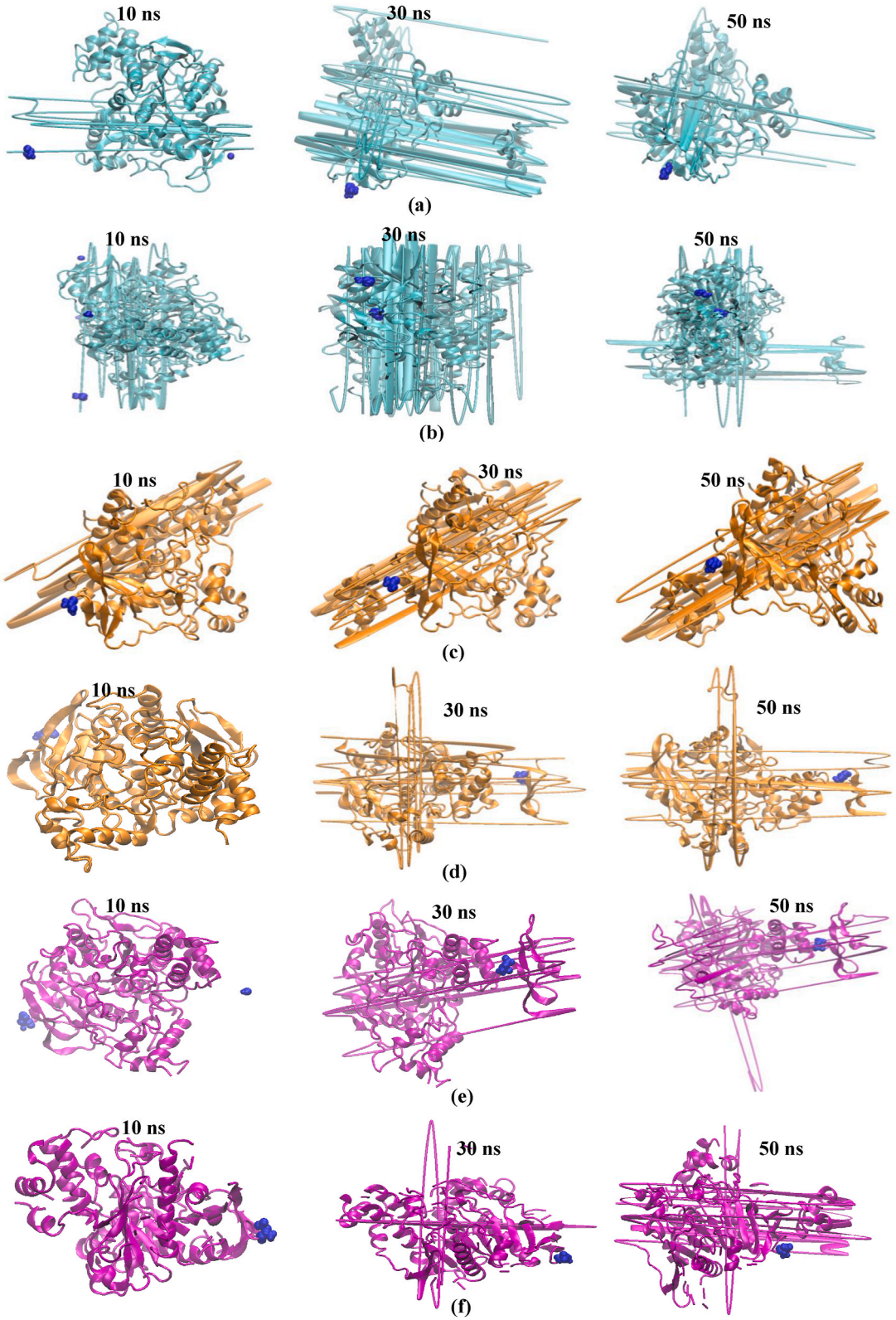


**Fig. 12.** Snapshots at different intervals (time step = 10, 30, 50 ns) for the binding modes of the ligand-protein complexes. The cartoon representation shows (a) 1GQR - 1,4,7,10,13,16-hexaoxacyclooctadecane, (b) 1GQR - tacrine, (c) 1QTI - butanoic acid, 3-methyl-2-[(phenylmethoxy) imino]-, trime, (d) 1QTI – tacrine, (e) 4PQE - butanoic acid, 3-methyl-2-[(phenylmethoxy)imino]-, trime and (f) 4PQE - tacrine complexes.

imino]-, trime; butane-1,2,3,4-tetraol; and D-(+)-ribonic acid.gamma-lactone as potent inhibitors of AChE from *C. spinosa* fruit extract demonstrated through docking studies. This is the first time that these compounds were reported for the AChE inhibitor. As a consequence, the combined results of the *in-silico* research using computational techniques may develop into potential new lead compounds against the chosen AD targets. H bond angles in the MD simulations were depicted in Fig. 11(a–f). Snapshots at different intervals (time step = 10, 30, 50 ns) for the binding modes of the ligand-protein complexes were generated to elucidate the position and binding modes of the ligands during the 50 ns MD simulation period shown in Fig. 12(a-f). The ligands are depicted as spheres, while the protein is depicted as a cartoon, and all ligands were observed to bind stably within the protein binding pocket.

## 5. Conclusions

The development of therapeutics for AD is significantly influenced by the cholinesterase enzyme AChE. This study investigates four potential compounds from C. spinosa fruit that may have anti-AD potential using *in silico* molecular modelling. The extraction processing conditions of extraction time – 60 min, the weight of powder – 6 gm, and volume of the solvent – 30 ml of Response Surface Methodology (RSM) optimization design we can get alkaloidal rich bioactive extracts from *C. spinosa* fruit. The first-line drug of Alzheimer's drugs tacrine and 90 compounds from *C. spinosa* were screened from the AChE target (1GQR, 1QTI and 4PQE) for possible therapy against AD using a ligand-based drug design and MD simulation approach. Drug likeness, ADMET analysis, and MD simulations (RMSD and RMSF) indicated their efficacy as drug molecules. These findings suggest that tacrine and the compounds from *C. spinosa* fruit have the potential to be effective in treating AD. Further studies should be conducted to validate their therapeutic effects and determine the optimal dosage for clinical use. From the above research, four compounds were found promising candidates for AChE inhibitor namely 1,4,7,10,13,16-hexaoxacyclooctadecane; butanoic acid, 3-methyl-2-[(phenylmethoxy)imino]-, trime; butane-1,2,3,4-tetraol; and D-(+)-ribonic acid.gamma-lactone as potent inhibitors of AChE.

To confirm the anti-AD potential of discovered drugs and get beyond computer analysis constraints, further laboratory and clinical research is needed. These investigations will provide a more thorough comprehension of the safety and effectiveness of the discovered compounds in the treatment of AD. The study provides insights into the binding of the AChE enzyme in AD, with future research focusing on anti-AD lead molecule isolation and *in vitro* AChE studies to further understand the mechanism of action and potential therapeutic targets. Additionally, exploring the efficacy of these lead molecules in animal models of AD could pave the way for future clinical trials and the development of novel treatments for this debilitating disease. These phytoconstituents are useful from the source of *C. spinosa* for the creation of novel AD medications that target the AChE, as they may be further altered and improved for better AD medications.

## Funding

This research did not receive any specific grant from funding agencies in the public, commercial, or not-for-profit sectors.

## CRediT authorship contribution statement

**Sathish T:** Writing – review & editing, Validation, Investigation. **Poovarasan R:** Investigation. **Tamizharasan G:** Investigation. **Abisek A:** Investigation. **Sulekha Khute:** Software, Methodology, Data curation, Conceptualization. **Kareti Srinivasa Rao:** Writing – review & editing, Software, Project administration, Formal analysis, Conceptualization. **Subash P:** Writing – review & editing, Writing – original draft, Visualization, Validation, Supervision, Methodology, Investigation, Data curation, Conceptualization.

## Declaration of competing interest

The authors declare that they have no known competing financial interests or personal relationships that could have appeared to influence the work reported in this paper.

## Acknowledgment

The authors express their gratitude to the Head of the Nanotechnology Research Center at the Department of Nanotechnology at the SRM Institute of Technology, Chennai, India, for providing a GC-MS facility.

## Appendix ASupplementary data

Supplementary data to this article can be found online at https://doi.org/10.1016/j.heliyon.2024.e27880.

## References

[1] A.A. Abduljawad, M.A. Elawad, M.E.M. Elkhalifa, A. Ahmed, A.A.E. Hamdoon, L.H.M. Salim, Alzheimer's disease as a major public health concern: role of dietary saponins in mitigating neurodegenerative disorders and their underlying mechanisms, Molecules 27 (20) (2022) 6804.

[2] T.C. Santos dos, T.M. Gomes, B.A.S. Pinto, A.L. Camara, A.M.D.A. Paes, Naturally occurring acetylcholinesterase inhibitors and their potential use for Alzheimer's disease therapy, Front. Pharmacol. 18 (2018) 9.
[3] S. Mitra, M. Muni, N.J. Shawon, R. Das, T.B. Emran, R. Sharma, Tacrine derivatives in neurological disorders: focus on molecular mechanisms and neurotherapeutic potential, Oxid. Med. Cell. Longev. 2022 (2022) 1–22.
[4] H. Allain, D. Bentue-Ferrer, O. Tribut, S. Gauthier, B.F. Michel, C.D.L. Rochelle, Alzheimer's disease: the pharmacological pathway, Fundam. Clin. Pharmacol. 17 (4) (2003) 419–428.
[5] Z. Ismail, B. Creese, D. Aarsland, H.C. Kales, C.G. Lyketsos, R.A. Sweet, Psychosis in Alzheimer disease — mechanisms, genetics, and therapeutic opportunities, Nat. Rev. Neurol. 18 (3) (2022) 131–144.
[6] R. Ullah, A.S. Alqahtani, O.M.A. Noman, A.M. Alqahtani, S. Ibenmoussa, M. Bourhia, A review on ethno-medicinal plants used in traditional medicine in the Kingdom of Saudi Arabia, Saudi J. Biol. Sci. 27 (10) (2020) 2706–2718.
[7] D. Timalsina, H.P. Devkota, D. Bhusal, K.R. Sharma, Catunaregam spinosa, Thunb Tirveng, A. Aspects, A. Iqbal (Eds.), EBCAM, 2021, pp. 1–10, 2021 (25).
[8] H. Saini, J. Dwivedi, H. Paliwal, U. Kataria, P. Chauhan, R. Garg, Anti-inflammatory, analgesic and antipyretic activity of catunaregam spinosa (thumb.), Tirveng Extracts JDDT 9 (5) (2019) 89–94.
[9] M.N.V. Gwedela, H. Terai, F. Lampiao, K. Matsunami, H. Aizawa, Anti-seizure effects of medicinal plants in Malawi on pentylenetetrazole-induced seizures in zebrafish larvae, J. Ethnopharmacol. 284 (2022) 114763.
[10] M. Varadharajan, Y. Sunkam, G. Magadi, D. Rajamanickam, D. Reddy, V. Bankapura, Pharmacognostical studies on the root bark and stem bark of Catunaregam spinosa (Thunb.) Tiruv. (Madanaphala) – an Ayurvedic drug, J. Complement. Med. Res. 4 (2) (2014) 89.
[11] V. Madhavan, S. Yoganarasimhan, M. Gurudeva, R. Deveswaran, D. Reddy, V. Bankapura, Pharmacognostical Studies on the Root Bark and Stem Bark of Catunaregam Spinosa (Thunb.) Tiruv. (Madanaphala)–An Ayurvedic Drug, 2014.
[12] D.M. Reddy, Pharmacognostical, Phytochemical and Sedative Activity Studies on the Root Bark of Catunaregam Spinosa (Thunb.) Tirven (Doctoral Dissertation, Rajiv Gandhi University of Health Sciences, India, 2011.
[13] K.D. Yang, Y.J. Li, L. Ge, Z.Z. Qin, Isolation of triterpenoids from catunaregam spinosa, Adv. Mater. Res. 236 (2011) 1731–1737.
[14] P.K. Lawrence, M.L.A.M.S. Munasinghe, W.T.P.S.K. Senarath, S. Suresh, Toxicity of methanolic extract of fruits of catunaregam spinosa (Rubiaceae) on Danio rerio embryos, J. Pharm. Res. Int 21 (2022) 33–41.
[15] A.N. Anoopkumar, S. Rebello, A.V. Sudhikumar, S. Puthur, E.M. Aneesh, A novel intervention on the inhibiting effects of Catunaregam spinosa induced free radical formation and DNA damage in Aedes aegypti (Diptera: Culicidae): a verdict for new perspectives on microorganism targeted vector control approach, Int. J. Trop. Insect Sci. 40 (4) (2020) 989–1002.
[16] Z. Yang, D. Zhang, J. Ren, M. Yang, S. Li, Acetylcholinesterase inhibitory activity of the total alkaloid from traditional Chinese herbal medicine for treating Alzheimer's disease, Med. Chem. Res. 21 (2012) 734–738.
[17] P.R. Bertelli, R. Biegelmeyer, E.P. Rico, L.C. Klein-Junior, N.S. Toson, L. Minetto, A.T. Henriques, Toxicological profile and acetylcholinesterase inhibitory potential of Palicourea deflexa, a source of β-carboline alkaloids, Comp. Biochem. Physiol. C Toxicol. Pharmacol. 201 (2017) 44–50.
[18] A. Dey, A. Mukherjee, Plant-derived alkaloids: a promising window for neuroprotective drug discovery, in: Discovery and Development of Neuroprotective Agents from Natural Products, 2018, pp. 237–320.
[19] S. López, J. Bastida, F. Viladomat, C. Codina, Acetylcholinesterase inhibitory activity of some Amaryllidaceae alkaloids and Narcissus extracts, Life Sci. 71 (21) (2002) 2521–2529.
[20] H. Teng, Y.H. Choi, Optimization of ultrasonic-assisted extraction of bioactive alkaloid compounds from nophel coptidis (Coptis chinensis Franch.) using response surface methodology, Food Chem. 142 (2014) 299–305.
[21] W. Huang, A. Xue, H. Niu, Z. Jia, J. Wang, Optimised ultrasonic-assisted extraction of flavonoids from Folium eucommiae and evaluation of antioxidant activity in multi-test systems in vitro, Food Chem. 114 (3) (2009) 1147–1154.
[22] I. Grigoriadis, Chern-Simons Topology Geometrics for the Generation of the RoccustyrnaTM Molecule, a Ligand Targeting COVID-19-SARS-COV-2 SPIKE D614G Binding Sites, 2020.
[23] S.K. Kondapuram, S. Sarvagalla, M.S. Coumar, Docking-based virtual screening using PyRx tool: autophagy target Vps34 as a case study, Molecular Docking for Computer-Aided Drug Design (2021) 463–477.
[24] N. Hamaamin Hussen, A. Hameed Hasan, J. Jamalis, S. Shakya, S. Chander, H. Kharkwal, Potential inhibitory activity of phytoconstituents against black fungus: in silico ADMET, molecular docking and MD simulation studies, Comput. Toxicol. 24 (2022) 100247.
[25] G.J. Swamy, A. Sangamithra, V. Chandrasekar, Response surface modeling and process optimization of aqueous extraction of natural pigments from Beta vulgaris using Box–Behnken design of experiments, Dyes Pigments 111 (2014) 64–74.
[26] S.K. Kondapuram, S. Sarvagalla, M.S. Coumar, Docking-based virtual screening using PyRx tool: autophagy target Vps34 as a case study, Molecular Docking for Computer-Aided Drug Design (2021) 463–477.
[27] P. Englebienne, N. Moitessier, Docking ligands into flexible and solvated macromolecules. 5. Force-Field-Based prediction of binding affinities of ligands to proteins, J. Chem. Inf. Model. 49 (11) (2009) 2564–2571.
[28] K.C. Hsu, Y.F. Chen, S.R. Lin, J.M. Yang, iGEMDOCK: a graphical environment of enhancing GEMDOCK using pharmacological interactions and post-screening analysis, BMC Bioinf. 12 (2011) 1–11.
[29] X. Chen, H. Li, L. Tian, Q. Li, J. Luo, Y. Zhang, Analysis of the physicochemical properties of Acaricides based on Lipinski's rule of five, J. Comput. Biol. 27 (9) (2020) 1397–1406.
[30] P. Sarker, A. Mitro, H. Hoque, M.N. Hasan, G.M.N.A. Jewel, Identification of potential novel therapeutic drug target against Elizabethkingia nopheles by integrative pan and subtractive genomic analysis: an in silico approach, Comput. Biol. Med. 165 (2023) 107436.
[31] R. Agrawal, H.B. Punarva, G.O. Heda, Y.M. Vishesh, P. Karunakar, VinaLigGen: a method to generate LigPlots and retrieval of hydrogen and hydrophobic interactions from protein-ligand complexes, J. Biomol. Struct. Dyn. 11 (2023) 1–4.
[32] A.G. Karabadzhak, L.M. Petti, F.N. Barrera, A.P.B. Edwards, A. Moya-Rodríguez, Y.S. Polikanov, Two transmembrane dimers of the bovine papillomavirus E5 oncoprotein clamp the PDGF β receptor in an active dimeric conformation, Proc. Natl. Acad. Sci. USA 114 (35) (2017) E7262–E7271.
[33] A. Singh, K. Singh, K. Kaur, A. Sharma, P. Mohana, J. Prajapati, U. Kaur, D. Goswami, S. Arora, R. Chadha, P.M. Bedi, Discovery of triazole tethered thymol/carvacrol-coumarin hybrids as new class of α-glucosidase inhibitors with potent in vivo antihyperglycemic activities, Eur. J. Med. Chem. 5 (263) (2024) 115948.
[34] A. Singh, H. Kaur, S. Arora, P.M.S. Bedi, Design, synthesis, and biological evaluation of novel morpholinated isatin–quinoline hybrids as potent anti-breast cancer agents, Arch. Pharmazie 355 (2) (2022) 2100368.
[35] J. Lee, X. Cheng, S. Jo, A.D. MacKerell, J.B. Klauda, W. Im, CHARMM-GUI input generator for NAMD, Gromacs, Amber, Openmm, and CHARMM/OpenMM simulations using the CHARMM36 additive force field, Biophys. J. 110 (3) (2016) 641a.
[36] S. Jo, J.B. Lim, J.B. Klauda, W. Im, CHARMM-GUI membrane builder for mixed bilayers and its application to yeast membranes, Biophys. J. 97 (1) (2009) 50–58.
[37] E.L. Wu, X. Cheng, S. Jo, H. Rui, K.C. Song, E.M. Dávila-Contreras, W. Im, CHARMM-GUI membrane builder toward realistic biological membrane simulations, J. Comput. Chem. 35 (27) (2014) 1997–2004.
[38] P. Eastman, J. Swails, J.D. Chodera, R.T. McGibbon, Y. Zhao, K.A. Beauchamp, L.P. Wang, A.C. Simmonett, M.P. Harrigan, C.D. Stern, R.P. Wiewiora, OpenMM 7: rapid development of high performance algorithms for molecular dynamics, PLoS Comput. Biol. 13 (7) (2017) e1005659.
[39] Y.P. Ng, T.C.T. Or, N.Y. Ip, Plant alkaloids as drug leads for Alzheimer's disease, Neurochem. Int. 89 (2015) 260–270.
[40] G. Marucci, M. Buccioni, D.D. Ben, C. Lambertucci, R. Volpini, F. Amenta, Efficacy of acetylcholinesterase inhibitors in Alzheimer's disease, Neuropharmacology 190 (2021) 108352.
[41] P. Camps, X. Formosa, C. Galdeano, T. Gómez, D. Muñoz-Torrero, L. Ramírez, Tacrine-based dual binding site acetylcholinesterase inhibitors as potential disease-modifying anti-Alzheimer drug candidates, Chem. Biol. Interact. 187 (1–3) (2010) 411–415.

[42] J. Kirchmair, P. Markt, S. Distinto, D. Schuster, G.M. Spitzer, K.R. Liedl, T. Langer, G. Wolber, The Protein Data Bank (PDB), its related services and software tools as key components for in silico guided drug discovery, J. Med. Chem. 51 (22) (2008) 7021–7040.
[43] E. Kellenberger, N. Foata, D. Rognan, Ranking targets in structure-based virtual screening of three-dimensional protein libraries: methods and problems, J. Chem. Inf. Model. 48 (5) (2008) 1014–1025.
[44] F. Anwar, U. Saleem, B. Ahmad, M. Ashraf, A.U. Rehman, M. Froeyen, L.Y. Kee, I. Abdullah, M.U. Mirza, S. Ahmad, New naphthalene derivative for cost-effective AChE inhibitors for Alzheimer's treatment: in silico identification, in vitro and in vivo validation, Comput. Biol. Chem. 1 (89) (2020) 107378.
[45] D.S. Prasanth, M.K. Shadakshara, S.F. Ahmad, R. Seemaladinne, M. Rudrapal, P.K. Pasala, Citronellal as a promising candidate for Alzheimer's disease treatment: a comprehensive study on in silico and in vivo anti-acetylcholine esterase activity, Metabolites 13 (11) (2023) 1133.
[46] H. Neuvirth, R. Raz, G. Schreiber, ProMate: a structure based prediction program to identify the location of protein–protein binding sites, J. Mol. Biol. 338 (1) (2004) 181–199.
[47] R.E. Hubbard, M.K. Haider, Hydrogen bonds in proteins: role and strength, eLS (2010) 1–7.
[48] K.C. Hsu, Y.F. Chen, S.R. Lin, J.M. Yang, iGEMDOCK: a graphical environment of enhancing GEMDOCK using pharmacological interactions and post-screening analysis, BMC Bioinf. 12 (2011) 1–11.
[49] K.S. Rao, P. Subash, In silico exploration of anti-Alzheimer's compounds present in methanolic extract of Neolamarckia cadamba bark using GC-MS/MS, Arab. J. Chem. 13 (7) (2020) 6246–6255.
[50] S.R. Kareti, P. Subash, In silico molecular docking analysis of potential anti-alzheimer's compounds present in chloroform extract of Carissa carandas leaf using gas chromatography MS/MS, Curr. Ther. Res. 93 (2020) 100615.
[51] A. Muthuraman, M. Ramesh, F. Mustaffa, A. Nadeem, S. Nishat, N. Paramakrishnan, K.G. Lim, In silico and in vitro methods in the characterization of beta-carotene as pharmaceutical material via acetylcholine esterase inhibitory actions, Molecules 28 (11) (2023) 4358.
[52] C. Bartolucci, E. Perola, C. Pilger, G. Fels, D. Lamba, Three-dimensional structure of a complex of galanthamine (Nivalin®) with acetylcholinesterase from Torpedo californica: implications for the design of new anti-Alzheimer drugs, Proteins: Struct., Funct., Bioinf. 42 (2) (2001) 182–191.
[53] A.K. Nivedha, D.F. Thieker, S. Makeneni, H. Hu, R.J. Woods, Vina-Carb: improving glycosidic angles during carbohydrate docking, J. Chem. Theor. Comput. 12 (2) (2016) 892–901.
[54] S. Rampogu, G. Lee, J.S. Park, K.W. Lee, M.O. Kim, Molecular docking and molecular dynamics simulations discover curcumin analogue as a plausible dual inhibitor for SARS-CoV-2, Int. J. Mol. Sci. 4 (3) (2022) 1771.
[55] S. Ravi, B. Priya, P. Dubey, V. Thiruvenkatam, S. Kirubakaran, Molecular docking and molecular dynamics simulation studies of quinoline-3-carboxamide derivatives with DDR kinases–selectivity studies towards ATM kinase, Chemistry 3 (2) (2021) 511–524.
[56] Q.H. Tran, Q.T. Nguyen, N.Q. Vo, T.T. Mai, T.T. Tran, T.D. Tran, M.T. Le, D.T. Trinh, K.M. Thai, Structure-based 3D-Pharmacophore modeling to discover novel interleukin 6 inhibitors: an in silico screening, molecular dynamics simulations and binding free energy calculations, PLoS One 6 (4) (2022) e0266632.
[57] M.M. Hasan, A.R.M. Shawon, A. Aeyas, M.A. Uddin, Cyclic peptides as an inhibitor of metastasis in breast cancer targeting MMP-1: computational approach, Inform. Med. Unlocked 35 (2022) 101128.
[58] W.M. Alaerjani, K.A. Khan, B.M. Al-Shehri, H.A. Ghramh, A. Hussain, M.E. Mohammed, M. Imran, I. Ahmad, S. Ahmad, A.S. Al-Awadi, Chemical profiling, antioxidant, and antimicrobial activity of Saudi propolis collected by Arabian honey bee (Apis mellifera jemenitica) colonies, Antioxidants 21 (7) (2022) 1413.